5-2007

Groundwater characterization at Yucca Mountain task 2: Surface complexation and solid phase sorption

Kenneth Czerwinski
University of Nevada, Las Vegas, czerwin2@unlv.nevada.edu

Anthony Hechanova
University of Nevada, Las Vegas

Amy J. Smiecinski
University of Nevada, Las Vegas, smiecins@unlv.nevada.edu

Nevada System of Higher Education

TECHNICAL REPORT

Title: Groundwater Characterization at Yucca Mountain
Task 2: Surface Complexation and Solid Phase Sorption

Report Document Identifier:

TR-06-006
Task ORD-RF-02

REVISION: 0

Author:	Ken Czerwinski	[redacted] (approval signature)	25-May-07 date
PI:	**Anthony Hechanova**	[redacted] (approval signature)	5/25/07 date
QA Manager:	**Amy Smiecinski**	[redacted] (approval signature)	5-25-07 date

Groundwater Characterization at Yucca Mountain
Task 2: Surface Complexation and Solid Phase Sorption

1. Table of Contents

Figures

Tables

Acknowledgements: Tyler Sullens, Jeanette Daniels, Lani Seamans – University of Nevada Las Vegas, Las Vegas, NV

2. Purpose

The purpose and scope of this report is to present an overview of the experiments, methods, results, and conclusions from research performed for the project "Groundwater Characterization at Yucca Mountain Task 2: Surface Complexation and Solid Phase Dissolution". The impact of surface complexation, alteration phase formation, and solution competition with metal ions on the solubility and speciation of actinide elements (U, Pu, Np) will be examined. In particular the role of iron (as Fe^{2+} and Fe^{3+}) and silicate (as SO_3^{2-}) concentrations on speciation, solubility, sorption, and secondary phase formation of actinides will be investigated. While a large body of literature exists on the interaction of actinides with iron and iron oxide phases, relatively little has been explored regarding the impact of silicates on actinide speciation. Therefore the role of silicates will be the main focus of the report, as it is the primary factor which meaningfully contributes to the enhanced understanding of actinide environmental speciation.

The described topics are examined through two main studies areas: formation of precipitates from solution phase species and sorption of dissolved species to solids. The main actinide ion species of interests are UO_2^{2+}, NpO_2^{+}, and Pu^{4+}. These species were selected based on their importance as components of spent nuclear fuel and their potential to form soluble species. The main component of spent nuclear fuel is uranium; neptunium is expected to have a high solubility due to its pentavalent oxidation state, and plutonium may form colloidal species [1]. The aqueous phase pH, Fe concentration, and SiO_3^{2-} concentration are varied. The role of Fe is of importance since canister corrosion may elevate aqueous levels of iron. Since the groundwater near the Yucca Mountain site is approaching saturation in silicate concentration, evaluation of this anion is deemed crucial. Furthermore, geochemical research at the Nevada Test Site has identified goethite and silicates as important geominerals, offering further motive for the investigation of iron oxides and silicates [2]. The role of pH is fundamental in dictating actinide and iron hydrolysis [3] and is evaluated to ascertain its importance in speciation in the presence of the other solution constituents. The project results will elucidate the relative importance of Fe and silicates in actinide speciation, in particular the formation of precipitates and subsequently sorbed species. The main focus will be on the role of silicate.

3. Quality Assurance

The data are collected under the NSHE Quality Assurance Program based on implementing procedures found at http://hrcweb.nevada.edu/qa/iplv.htm. No conclusions of this Report are based on unqualified data.

4. Introduction

4.1. Overview of actinide environmental speciation

There has been a large effort to evaluating Np, Pu, and other actinide species present in the environment [4-7]. The important actinide phases and processes in the environment have been identified: precipitation, sorption, complexation, and colloid formation. The papers also stress that speciation dictates the environmental behavior of the actinides, allowing an analysis of mobility, toxicity, and risk. The main methods for

actinide immobilization in the environment are precipitation and sorption to geological surfaces. The combination of chemical kinetics and thermodynamics with site geochemistry in the evaluation of actinide environmental sorption has been shown to permit modeling for transport analysis and remediation activities over site variations [8]. Sorption of actinides to local sediment and solid phases is known to be a crucial control of their transport and environmental behavior. Actinide precipitation and sorption is highly influenced by local chemical conditions, in particular pH, solution phase composition, and Eh, in addition to the composition of the sediment. Due to these differing parameters, actinide sorption to sediment can be spatially varied at a given site.

A number of studies have been performed on the sorption of Np and Pu to sediments. The sorption and speciation of Pu to tuff has been studied by XAFS [9]. Plutonium was found to be sorbed to manganese oxides and clay smectites, but not iron oxides. The oxidation states of Pu were found to be hexa- and pentavalent. This work initiated further studies on the role manganese oxide on Pu sorption. Other studies have indicated differences between the sorption of Np and Pu [10]. In this study the sorption of Np can be described with a Freundlich isotherm, while Pu sorption does not exhibit such behavior under the examined conditions. Differences in the sorption sites are also expected, which can be attributed to the differing oxidation states of Np and Pu used in the study. Unlike studies with tuff, this study found Pu sorbed to iron oxides. Again this can be traced to the Pu oxidation state, indicating its dominant role in the environmental behavior of Pu and the need to understand actinide redox when evaluating and modeling sorption. These contradictions in the role of iron oxides for Pu sorption are important regarding near field corrosion of containers in evaluation sorption behavior.

Batch experiments have been used to examine the Np redox species involved in sorption to iron oxides [11-13]. The techniques included EXAFS, solvent extraction, and XPS. Modeling was performed to determine complexation constants and the influence of carbonate on speciation and Np sorption behavior was observed. Surface properties of the oxides were found to influence Np sorption. The sorption of Np to clay phases has also been examined [14-17]. The role of pH and carbonate concentration has been evaluated with carbonate species shown to compete with surface sorption. The formation of the Np hydroxide species has been correlated with sorption, indicating an important role in solution speciation on the sorption behavior of Np. This indicates speciation modeling of Np and Pu can aid in sorption evaluation, since the solution chemistry will dictate the formation of carbonate, hydroxide, or mixed hydroxycarbonate species.

4.2. Actinide interaction with silicates

Previous studies have explored the sorption of uranyl and neptunyl on silicates and iron oxides [18]. Competitive ligands were shown to influence sorption and were strongly linked to pH. The formation of carbonate species above pH 8 was demonstrated to increase uranyl solution concentration due to the formation of soluble carbonate species. The sorption of uranyl on zirconium silicates and oxides has been examined [19]. These results are expected to differ from the iron system due to fundamental variation between Fe and Zr chemistry, but they provide a useful comparison. These data have been used to link structural evaluation of the sorbed species with modeling, particularly in developing species constraints in the system. Neptunium chemistry in silicate gels has been studied for different oxidation states [20]. Sorption of both

pentavalent and hexavalent oxidation states was observed, with high sorption for Np(V). Organic ligands were shown to reduce the sorption of Np to the silicate gel. The complexation constants for the Np-organic species were accurately used to describe the degree of Np desorption due to the ligand. The results from the Np and U silicate studies provide support for the use of complexation data in evaluating expected speciation.

The influence of silicates on Pu speciation has been studied in solution and solid phases. Tetravalent Pu interaction with Na_2SO_3 was examined from pH 9 to 14 [21]. The Pu silicate species in solution were determined between pH 11 and 13.8, with the expected species due to complexation of the SiO_3^{2-} anion. At pH 9 no effect of SiO_3^{2-} on Pu solubility was observed. These results indicate that silicon solution species will have no influence in the formation of soluble Pu species except above pH 9. In silicate waste forms with Pu, corrosion was shown to induce a silicate phase with high Pu concentration [22]. This observation was used to propose the potential formation of Pu secondary phases due to interaction of original waste forms with the high silicate water near Yucca Mountain. Plutonium silicate phases are expected to be stable and have been investigated as nuclear waste forms [23].

4.3. Speciation and environmental behavior

A range of methods can be employed in assessing environmental speciation and behavior. At very small scales, atomistic simulation can provide detailed information on surface behavior. However, this description is limited to systems with thousands of atoms. As the modeling scale increases, and different sorption sites are included, a distribution of surface complexation constants can be employed. Continuum-level models include isotherms and surface complexation models. The isotherms can be described by both linear and non-linear terms and may not reflect the actual chemistry on the surface. Models that describe surface complexation [24] are based on the functional chemistry operating at the surface. A composite approach to modeling is based on molecular-level information but considers the surface to be undifferentiated with respect to mineral surface site type [25], using weak and strong sites to describe differences in functional groups. The component additivity approach is formulated on the concept that sorption is the sum of the interacting functional groups, or sites on the surface [26].

Fundamental environmental speciation using chemical kinetics and thermodynamics is known to be extremely useful and relevant in evaluating chemical forms. A schematic representing reactions and accompanying constants is shown in Figure 1**.** Chemical description by this method permits the inclusion of data into a variety of models [27], improving and extending its utility.

The complexation constants and kinetic terms can be generated from fundamental chemical reactions. A general chemical reaction is described as:

$$aM^{z+} + bL^{x-} \Leftrightarrow M_aL_b^{(az-bx)} \qquad \text{Eq. 1}$$

for complexation or

$$M_aL_{b(s)} \Leftrightarrow aM^{Z+} + bL^{x-} \qquad \text{Eq. 2}$$

for the solubility of a solid where M is the metal ion and L is a ligand. The kinetics of the reaction can be measured to establish time conditions needed to reach equilibrium. The change in radionuclide and ligand concentration can drive the formation of various chemical species.

Figure 1. Environmental reactions and the accompanying constants

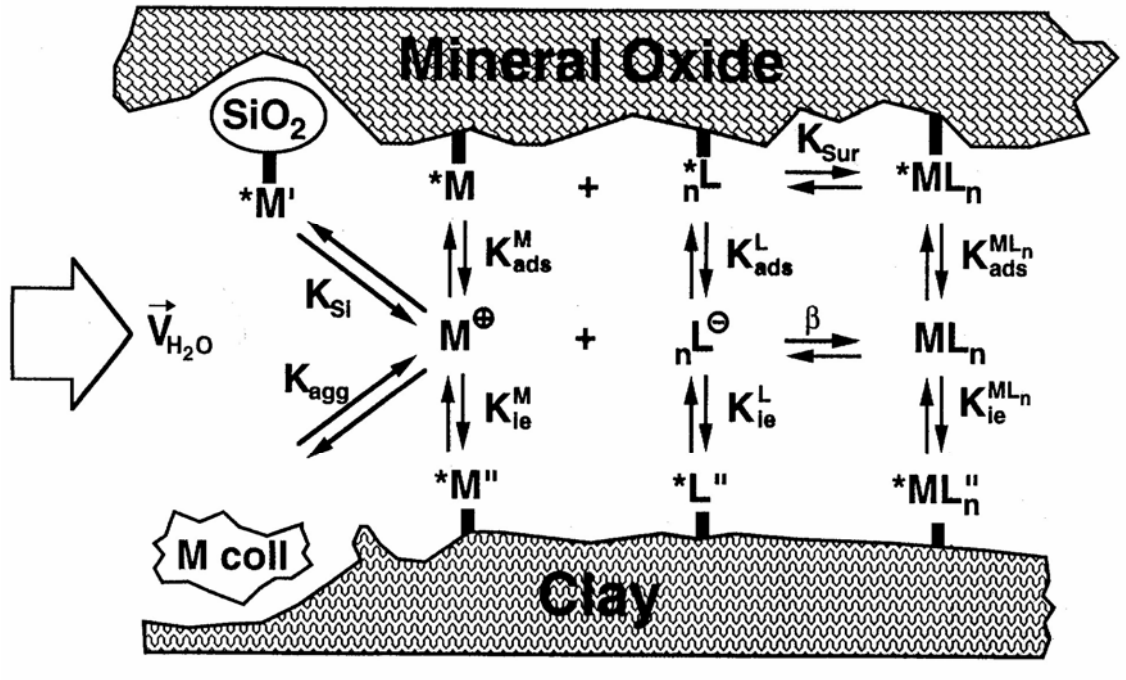

Non-Q for informational purposes only

From Eq. 1, the stability constant to describe speciation at equilibrium can be evaluated as:

$$\beta_{M_aL_b} = \frac{\gamma_{M_aL_b}\left[M_aL_b^{(az-bx)}\right]}{\gamma_M\left[M^{Z+}\right]^a\gamma_L\left[L^{x-}\right]^b} \quad \text{Eq. 3}$$

and, from Eq. 2, the solubility constant:

$$\mathrm{K}_{sp(M_aL_b)} = \gamma_M\left[M^{Z+}\right]^a\gamma_L\left[L^{x-}\right]^b \quad \text{Eq. 4}$$

The activity coefficients are denoted by γ. If the constants are measured as a function of ionic strength, the specific ion interaction theory or the Pitzer equation can be used to evaluate constants at different ionic strengths. Temperature variations are explained by second law extrapolations with the Gibbs free energy. Enthalpy and entropy are investigated by evaluating the stability constant as a function of temperature through the following equations (using standard nomenclature) [28]:

$$\Delta G = -RT\ln\beta \quad \text{Eq. 5}$$

$$R\ln\beta = -\frac{\Delta H}{T} + \Delta S \quad \text{Eq. 6}$$

Kinetic data on solid phase dissolution or sorption can be found by evaluating solution concentration as a function of time. Kinetics analyses can be used to determine dissolution rate constants, surface area mass normalized dissolution, and solution equilibrium conditions. Dissolution rate constants can be determined with the equation below [29]:

$$\left[M\right]_t = \left[M\right]_{eq}\left(1-e^{-kt}\right) \quad \text{Eq. 7}$$

where $[M]_t$ is the examined metal ion solution concentration at time *t*, $[M]_{eq}$ is the metal solution concentration at equilibrium, and *k* is the rate constant in inverse time units. Sorption rates constants can use the equation

$$[M]_t = [M]_{eq} + [M]_{sorb}\left(e^{-kt}\right) \quad \text{Eq. 8}$$

where the additional term $[M]_{sorb}$ is the maximum concentration of sorbed metal ion. The decrease in concentration due to radioactive decay can be accounted for with substitutions into the above equations.

5. Methods and materials

All materials and standards used conformed with QA requirements. Experiment procedures used are from IPLVs and are at http://hrcweb.nevada.edu/qa/iplv.htm. The IPLVs used in this work shown in Table 1.

Table 1. IPLVs used in this study.

IPLV-003 rev. 3 Analytical and Top Loading Balance Use
IPLV-005 rev. 1 Batch Testing
IPLV-012 rev. 3 Measurement of Conductivity, Alkalinity, and pH in Water Samples
IPLV-017 rev. 2, 3 Pipettor Use and Calibration Check
IPLV-071 rev. 0 Measurement of Aqueous Constituent Concentrations by Inductively Coupled Plasma Atomic Emission Spectroscopy (ICP-AES) or Inductively Coupled Plasma Mass Spectroscopy (ICP-MS)
IPLV-072 rev. 0 Measurement of Radionuclide Activity by Liquid Scintillation counting (LSC)
IPLV-078 rev. 0 Use of Ultraviolet Visible Spectrometer
IPLV-079 rev. 0 Determination of Surface Area of Solid Samples

The studies include data collected under QA protocols as well as data that did not conform to QA requirements (Table 2). The experiments performed in this study can be divided into precipitation and sorption experiments. The experimental approach used in the project is shown below and demonstrates the areas of research as well as the techniques employed.

Table 2. QA and non-QA project methods and data. The method abbreviations are defined below the table.

Precipitation studies		**Sorption studies**	
QA methods	**Non-QA method**	**QA methods**	**Non-QA method**
Sample preparation	Colloidal studies	Sample preparation	XRD
pH measurement	SEM/EDAX	pH measurement	SEM/EDAX
ICP-AES	IR spectroscopy	LSC	SAA
UV-Visible Ferrozine for Fe^{2+}	XAFS		LA-ICP-MS

ICP-AES: Inductively coupled plasma-atomic emission spectroscopy; XAFS: X-ray absorption fine structure spectroscopy; SEM/EDAX: Scanning electron microscopy/Energy dispersive X-ray analysis; XRD: X-ray diffraction; IR spectroscopy: Infrared spectroscopy; LSC: Liquid scintillation counting; SAA: Surface area analysis; LA-ICP-MS: Laser ablation inductively coupled plasma mass spectroscopy.

Figure 2. Overview of experimental approach and techniques.

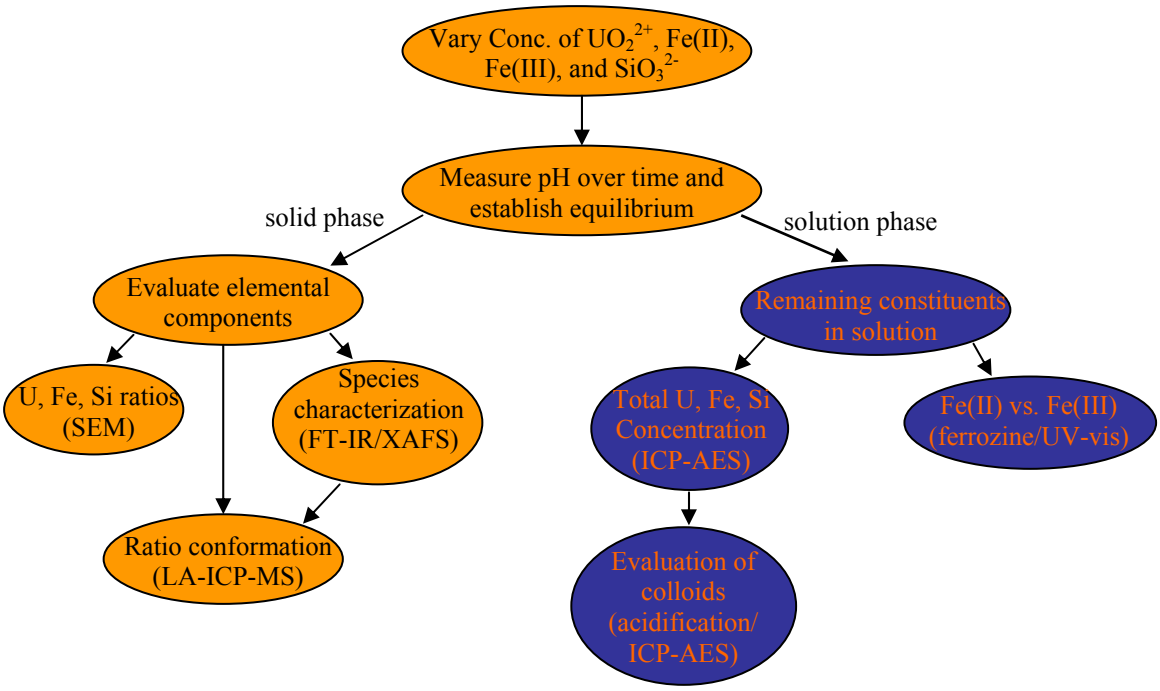

Non-Q for informational purposes only

5.1. Precipitation experimental conditions and methods

The sample preparation for the precipitation experiments utilized the following IPLVs

- IPLV-003 rev. 3 Analytical and Top Loading Balance Use
- IPLV-012 rev. 3 Measurement of Conductivity, Alkalinity, and pH in Water Samples
- IPLV-017 rev. 2, 3 Pipettor Use and Calibration Check

Stock solutions were prepared at 50 mM of each of $UO_2(NO_3)_2$, Na_2SiO_3, and $FeCl_3$ and 37.5 mM for $FeCl_2$. Samples were prepared with a total volume of 45 mL and the component solution concentration of uranyl, silicate, Fe^{2+}, and Fe^{3+} was varied at 0, 0.1, and 1 mM for each component. A large matrix was required to evaluate all the conditions. The stock solutions were added in the order U, Fe(II), Fe(III), and SiO_3^{2-} to water initially set at pH 6.0, 7.5, and 9.0 to prepare the 45 mL experimental samples. The solutions were equilibrated with normal atmosphere and the pH periodically measured. Equilibrium was defined by the stabilization of the pH. At equilibrium the solution phase concentration of U, Fe, and Si was determined with a Spectro CIROS CCD ICP-AES using IPLV-071 rev. 0.

The presence of colloids was examined by diluting collected samples with water or nitric acid. The difference between acid dilution and water dilution followed by filtering should indicate the presence colloids. Because colloids will dissolve in acid but not water, the concentration of colloids can be determined by the difference between the acid treated and water treated samples. The sample preparation methods for the colloid studies are below.

Set 1. 4.9 mL of each of the matrix solutions were transferred to a vial
0.1 mL of 1.6 M nitric acid was added to each of these solutions
5.0 mL of DI H_2O was added and the solutions mixed
Set 2. 5.0 mL of each of the previous solutions were transferred to a vial
5.0 mL of DI H_2O was added and the solutions mixed
Only the initial pH 6.0 solutions were measured on the ICP-AES with little to no indication of colloidal formation.
The concentration of Fe^{2+} in solution was determined by UV-visible analysis on the Varian Cary 6000i UV-Visible-NIR spectrometer with a ferrozine indicator by measuring absorbance at 560 nm. The IPLVs used for this method were IPLV-003 rev. 3, IPLV-017 rev. 2 and 3, and IPLV-078 rev. 0. A stock solution of ferrozine was prepared by mixing 20 mL of 7 mM ferrozine, 360 mL of H_2O, and 400 mL of 4.0 Buffer. To determine the Fe^{2+} concentration, 0.1 mL of each sample's solution phase was added to 3.9 mL of ferrozine stock solution. A calibration curve was prepared similarly from NIST standards.

After the evaluation of the solution phase species the samples were examined for precipitates. Each of the solutions with observable amounts of precipitate were centrifuged at 5000 rpm for 10 minutes. The aqueous phase was decanted and the remaining solid freeze-dried. A portion of the remaining solid was placed on an aluminum stub fitted with carbon conductive tape. Each sample was analyzed for U, Fe, and Si, with relative ratios provided using EDAX on a JEOL JSM-5610 SEM. Samples were also prepared for IR spectroscopy by pressing KBr pellets with approximately 1-5 wt % sample. The samples analyzed by IR were selected based on the ratios of each constituent indicated by EDAX. The peak descriptions were interpreted from literature data.

Samples used for XAFS were chosen form those solutions that produced sufficient precipate. Each sample was diluted with boron nitride to approximately 1 wt% uranium and spectra were recorded in fluorescence mode at BESSRC-CAT 12-BM beam line using a 13 element germanium detector. Uranium L_{III} edge (17,166 eV) X-ray absorption spectra were collected at the Advanced Photon Source using a Si (1,1,1) double crystal monochromator.. Use of the Advanced Photon Source was supported by the U. S. Department of Energy, Office of Science, Office of Basic Energy Sciences, under Contract No. DE-AC02-06CH11357.

Energy calibration was done using an Yttrium foils (K edge = 17,038 eV). For each sample, several EXAFS spectra were recorded at k = [0 - 12] $Å^{-1}$ and averaged. The background contribution was removed using Autobk software and data analysis was performed using WINXAS. For the fitting procedure, amplitude and phase shift function were calculated by FEFF8.2. The feff.inp files were generated by ATOMS using crystallographic structures taken from literature. The adjustments of EXAFS spectra were performed under the constraints S02 = 0.9, a single value of energy shift $\Delta E0$ was used for all scattering. The uncertainty on the coordination number (C.N) is 20%, the uncertainty on the distance (R) is 0.02 Å. A UO_2 XANES spectrum was recorded for U(IV) reference.

5.2. Sorption experimental conditions and methods

The sorption of the tracer isotopes $^{237}Np(V)$and $^{239}Pu(VI)$ to solid phases was examined in this task. The initial solution concentration of actinide tracer was 750 Bq/mL, resulting in $[Np]_0=1.21E^{-4}$ M and $[Pu]_o= 1.37\ E^{-6}$ M. Solid phases included core cutting from Yucca Mountain (SPC02043307 Virtual Box 01006942) and 200 mesh iron. Solution phases included DI H_2O, 1 mM SiO_3^{2-}, and J-12 water. The experimental samples were prepared by adding Np or Pu tracer to enough solution to yield a total volume of 500 mL then placing 100 g of solid phase in the solution. Samples were also prepared without solid phases. The solution pH evolved based on the interaction of the solution phase with the solid matrix and the atmosphere.

Solution pH and dissolved actinide concentration was evaluated over time. The pH was evaluated based on IPLV-012 rev. 3. The solution phase Np and Pu concentration was determined by liquid scintillation counting based on IPLV-072 rev. 0. The scintillation samples were prepared with 1.0 mL of aqueous phase from each sample added to 19.0 mL of Ultima Gold LSC cocktail. All samples were in polyethylene scintillation vials at room temperature. The LSC measured total counts 0-2000 KeV with counting ended at 2% σ or 90 minutes.

The solid phases from these studies were examined by XRD, EDAX, and SAA. The XRD analysis was performed on core raw sample and 200 mesh iron. The core raw sample indicated the presence of Fe metal from the drilling. The Fe metal was magnetically removed. Each diffraction pattern was collect from 10 to 90° 2θ. The EDAX samples were prepared by placing samples on an aluminum stub fitted with carbon conductive tape. Each sample was analyzed for Na, K, U, Fe, and Si, with relative ratios given. The surface area for unreacted 200 mesh iron, unreacted core raw, 200 mesh iron reacted with J-12 water, and core raw reacted with J-12 water were measured using the standard BET method. The measurements did not pass the QA requirements and is therefore non-Q.

6. Assumptions

A key assumption in the project design is the use that the silicate species prevalent at Yucca Mountain is SiO_3^{2-}. This assumption is based on the composition of J-13 water [30] (Table 3). The silicon concentration is reported at total aqueous and not as the direct species. From the solution phase data, the constituents at highest concentration in J-13 water are Na^+ and aqueous Si. The concentration ratio of these species is Na:Si = 2:1, indicating a anionic charge of 2^- for the silicate species to maintain charge neutrality. Even when cationic and anionic strengths are considered, to balance the charge of sodium the 1.015 mM Si must have a charge of -1.778, approximating the SiO_3^{2-} anion.

This task used J-12 groundwater rather than J-13. It is assumed the chemical composition of the ground water from both wells is similar.

In data analysis for the ion K values (Eq. 9), solution ion concentrations with values above the initial concentrations are set to the initial ion concentration. Solution ion concentrations with values below the MDL are set to the respective MDL to permit the determination of a real number when the data is input into Eq. 9.

Table 3. Chemical composition of J-13 ground water. [30]

Variable	Composition (mg/L)	mmol/L
Na^+	45.8	1.992
Cl^-	7.14	0.201
Si (aq)	28.5	1.015
Ca^{2+}	13	0.324
K^+	5.04	0.129
Mg^{2+}	2.01	0.084
Li^+	0.048	0.007
F^-	2.18	0.115
NO_3^-	8.78	0.142
SO_4^{2-}	18.4	0.192
pH	6-9	

Non-Q for information only

7. Results and Conclusions

The project results are presented below. The precipitation data provides the change in pH with time, solution phase concentration, and solid phase characterization. Sorption data is provided for Np and Pu interaction with the differing solutions and matrices. The project data can be accessed at http://hrcweb.nevada.edu/data/tda/ and is identified as ORD-RF-02. The results will be used to develop conclusions on the impact of silicate on actinide speciation under the examined conditions.

7.1. Results from pH analysis of precipitation data

The initial pH of the solutions for the precipitation experiments was 6.0, 7.5, and 9.0, with 84 samples prepared at each pH to evaluate the range of solution phase ion concentrations. No attempt was made to stabilize the pH. This resulted in the establishment of equilibrium based upon the initial solution conditions and a change in pH with time. Most solutions were stabilized within 790 hours, but variations were observed with pH (Table 4).

Table 4. Final pH of samples prepared for precipitation experiments.

Initial solution pH	Time to equilibrium (hours)	Minimum pH	Maximum pH
6.0	785	2.45	8.35
7.5	431	2.30	10.25
9.0	310	2.49	10.42

Data from R02JD.005, R02JD.006, and R02JD.007

7.2. Results from solution phase analysis

The numerous experimental samples show the conditions responsible for the largest relative reduction in solution phase solution phase ion concentration. Since the results

presented in Table 4 show a large pH overlap range regardless of initial solution conditions, the data from the differing starting pH values can be combined in examining ion speciation. The relative value for the solid phase concentration is found from

$$K_1 = \frac{[I]_{solid}}{[I]_{aq}} = \frac{[I]_o - [I]_{aq}}{[I]_{aq}} \qquad \text{Eq. 9}$$

where *I* represents the ions uranyl, total iron, or silicate, with $[I]_o$ the initial ion concentration. The data for iron includes both the divalent and trivalent oxidation states.

Table 5. Calculated K values for Fe from precipitation data. Concentrations are mM.

Sample ID	K_{Fe}	pH final	$[Fe^{3+}]_o$	$[Fe^{2+}]_o$	$[Si]_o$	$[U]_o$
TS-QA2-9-47	15.705	5.67	0	0.735	1	0.1
TS-QA2-9-23	14.286	5.31	0.1	0.735	1	0
TS-QA2-7.5-20 Dup	6.446	5.07	0	0.735	1	0
TS-QA2-7.5-20	5.744	4.90	0	0.735	1	0
TS-QA2-9-50	5.458	4.90	0.1	0.735	1	0.1
TS-QA2-7.5-68	2.943	4.83	0.1	0.0735	1	1
TS-QA2-9-12	2.943	6.74	0.1	0.0735	0	0
TS-QA2-9-13	2.943	6.92	0.1	0.0735	0.1	0
TS-QA2-9-39	2.943	5.10	0.1	0.0735	0	0.1
TS-QA2-9-40	2.943	6.39	0.1	0.0735	0.1	0.1

Data from R02TS.001 worksheet "K Values", R02JD.006, and R02JD.007

Table 6. Calculated K values for Si from precipitation data. Concentrations are mM.

Sample ID	K_{Si}	pH final	$[Fe^{3+}]_o$	$[Fe^{2+}]_o$	$[Si]_o$	$[U]_o$
TS-QA2-6-10	0.617	4.50	0	0.0735	0.1	0
TS-QA2-6-47	0.457	4.45	0	0.735	1	0.1
TS-QA2-7.5-20 Dup	0.428	5.07	0	0.735	1	0
TS-QA2-6-20 Dup	0.426	4.41	0	0.735	1	0
TS-QA2-9-50	0.419	4.90	0.1	0.735	1	0.1
TS-QA2-9-47	0.399	5.67	0	0.735	1	0.1
TS-QA2-6-20	0.384	4.41	0	0.735	1	0
TS-QA2-7.5-20	0.371	4.90	0	0.735	1	0
TS-QA2-7.5-47	0.349	4.65	0	0.735	1	0.1
TS-QA2-9-23	0.343	5.31	0.1	0.735	1	0

Data from R02TS.001 worksheet "K Values", R02JD.005, R02JD.006, and R02JD.007

The highest K_{Fe} values are for relatively high initial Fe(II) solution concentrations (Table 5) with a solution pH between 5 and 7. There are also relatively large initial concentrations of Si. For Si the highest K_{Si} values are center around pH 5 (Table 6). The initial conditions that trend with these high K_{Si} values are high initial Si concentration (1 mM) and the presence of Fe(II). The highest values are all below 1, indicating the bulk of the Si remains in solution phase under the experimental conditions. There is no clear trend for K_{Si} with U. The correlation with Fe^{2+} solution indicates silicates can form secondary phase in the presence of corroding Fe at pH near 5. For U the highest K_U tend to be near pH 7 and are independent of other solution ion concentrations, indicating the

importance of hydrolysis. The total U concentration for the highest values is 0.1 mM. Silicates show an importance in forming precipitates near pH 5.

Table 7. Calculated K values for U from precipitation data. Concentrations are mM.

Sample ID	K_U	pH final	$[Fe^{3+}]_o$	$[Fe^{2+}]_o$	$[Si]_o$	$[U]_o$
TS-QA2-9-27	1.326	7.29	0	0	0	0.1
TS-QA2-9-30	1.326	6.45	0.1	0	0	0.1
TS-QA2-9-36	1.326	6.93	0	0.0735	0	0.1
TS-QA2-9-47	1.326	5.67	0	0.735	1	0.1
TS-QA2-9-40	1.326	6.39	0.1	0.0735	0.1	0.1
TS-QA2-9-40 Dup	1.326	6.65	0.1	0.0735	0.1	0.1
TS-QA2-9-31	1.326	7.32	0.1	0	0.1	0.1
TS-QA2-7.5-28	1.326	6.90	0	0	0.1	0.1
TS-QA2-9-50	1.025	4.90	0.1	0.735	1	0.1
TS-QA2-7.5-47	0.991	4.65	0	0.735	1	0.1

Data from R02TS.001 worksheet "K Values", R02JD.006, and R02JD.007

The K values as determined from Eq. 9 can be used to evaluate the correlation of uranium speciation with the solution ion species by plotting K_U against K_{Fe} or K_{Si}. Based on the data in Table 7 the uranium data should be grouped based on its initial uranium concentration. However, even with the focusing of the dataset the broad pH variation in the samples should result in a spread of the data.

Figure 3. K_U vs. K_{Fe} for samples with 1.0 mM initial uranium solution concentration.

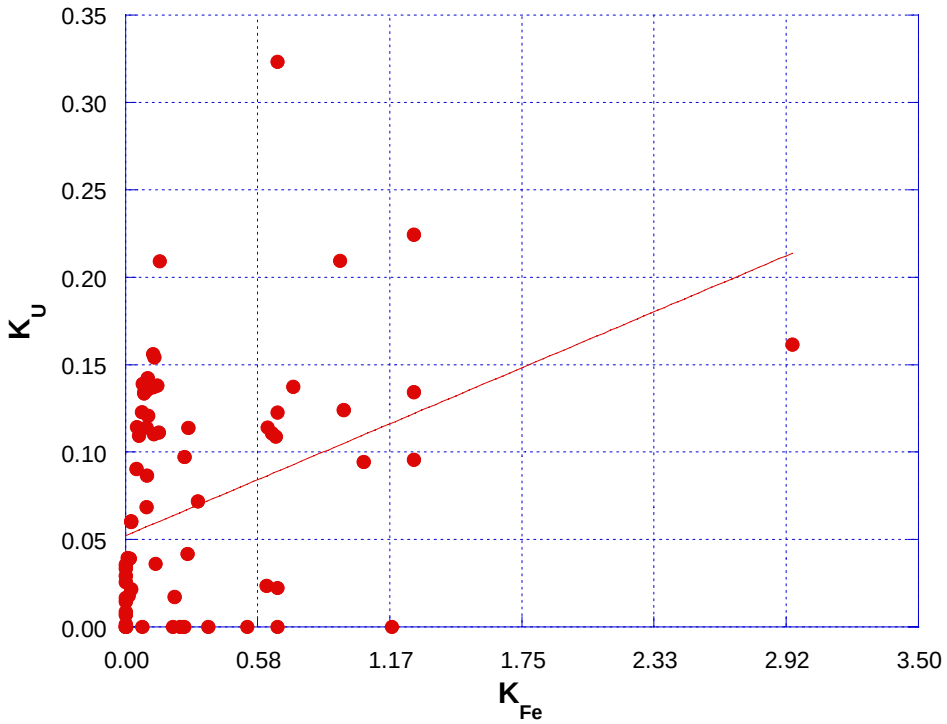

Data from R02TS.001 worksheet "K Values"

Figure 4. K_U vs. K_{Fe} for samples with 0.1 mM initial uranium solution concentration.

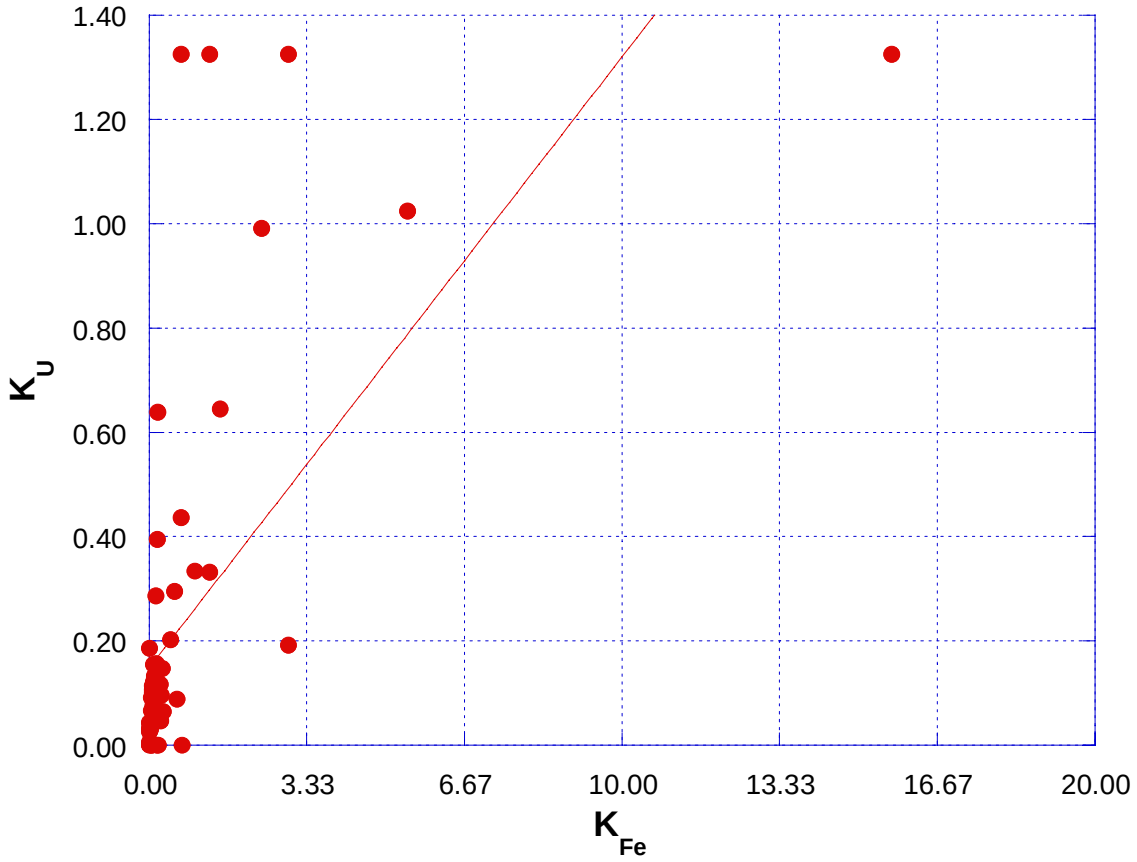

Data from R02TS.001 worksheet "K Values"

No correlation is observed for the relationship between U and Fe (Figure 3). The correlation coefficient value for the graph is 0.37 (R02TS.001 Worksheet "Correlation") from the least squares fit of the data suggesting no relationship between Fe and U speciation in the examined systems. The data for the K_U correlation with K_{Fe} at 0.1 mM total U (Figure 4) also does not provide any evidence of a relationship and has correlation coefficient value of 0.61 (R02TS.001 Worksheet "Correlation").

Unlike the analysis with K_{Fe}, a correlation is demonstrated when plotting K_U against K_{Si}. For a total uranium initial concentration of 1 mM (Figure 5), the correlation coefficient is 0.75 (R02TS.001 Worksheet "Correlation"), which is strong considering the large pH range evaluated. The slope is 0.84 ± 0.10 (R02TS.001 Worksheet "Correlation"), which designates a linear relationship between Si and U. The examination of the same correlation for 0.1 mM total initial uranium shows a correlation coefficient of 0.71 (R02TS.001 Worksheet "Correlation"), but with a slope of 1.51 ± 0.22 (R02TS.001 Worksheet "Correlation"). Under the examined conditions, a high solution phase concentration of silicate should result in a high uranium solution phase concentration. Conversely, precipitation of silicates should result in the formation of uranium solid phases.

Figure 5. K_U vs. K_{Si} for samples with 1 mM initial uranium solution concentration.

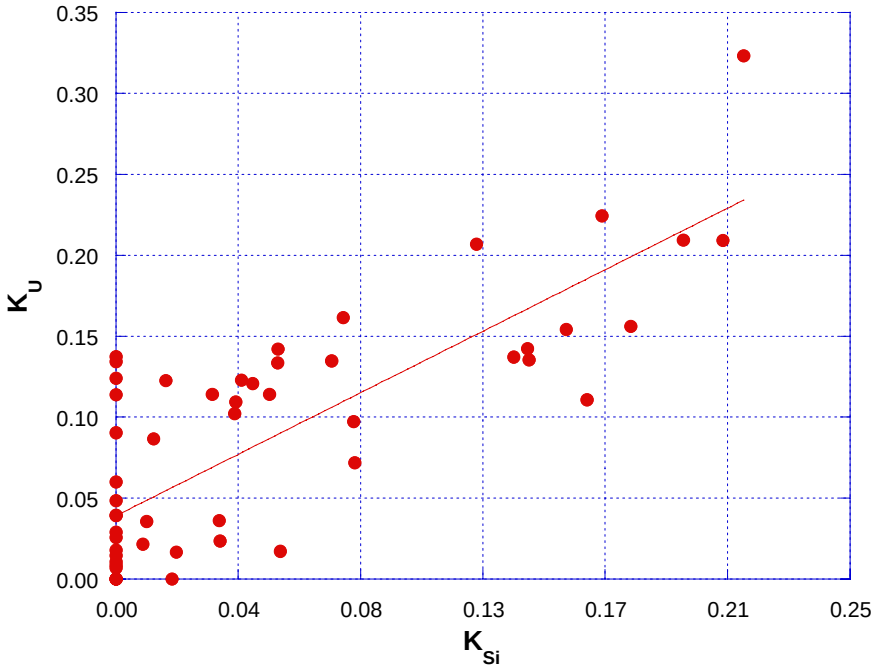

Data from R02TS.001 worksheet "K Values"

Figure 6. K_U vs. K_{Si} for samples with 0.1 mM initial uranium solution concentration.

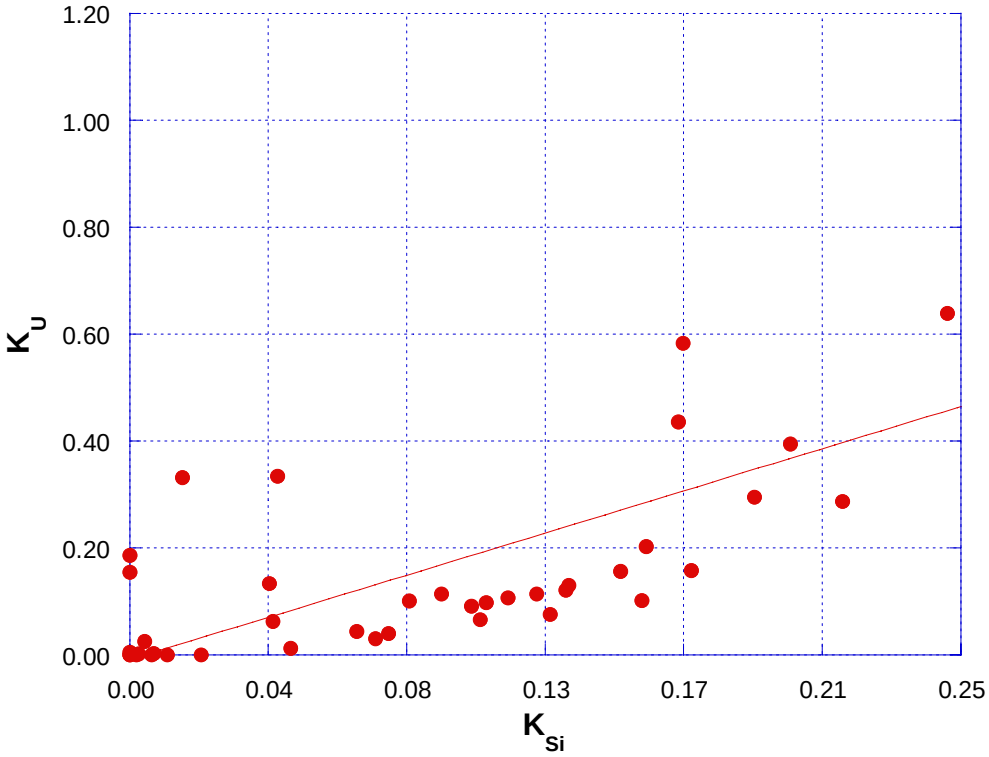

Data from R02TS.001 worksheet "K Values"

7.3. Results from solid phase analysis

Solid resulting from the precipitation experiments were examined by IR spectroscopy, SEM/EDAX, and XAFS. The data are useful in determining relative elemental concentrations, functional groups, and structural information. The samples examined by these methods are listed in Table 8.

7.3.1. EDAX analysis of solid phases

The precipitates with the highest relative elemental concentration for each of Fe, Si, and U are listed in Table 8. From the EDAX analysis the highest Si percentage was near 50 mol%. The seven samples in this range all had an initial silicate concentration of 1 mM in addition to the presence of U. The final pH values of these solutions are below 5.75. For Fe, the bulk of the samples examined by EDAX have atomic Fe elemental percentages between 20 mol% and 30 mol%. The four samples with the highest Fe percentages are between 80 mol% and 90 mol%. These high Fe containing precipitates result from solution with total Fe concentration at or above 1 mM and in the pH range near 2.5. Uranium-containing precipitates reach an atomic elemental percentage of 35 ± 2 mol%, with the remaining samples exhibiting around 10 mol% U. The five high U samples have either high K_U values or have 1 mM solution phase U concentration in the presence of 1 mM silicate.

Table 8. Precipitation samples resulting in solids examined by IR and EDAX. Initial concentrations are in mM.

Sample Name	pH final	$[Fe^{2+}]_o$	$[Fe^{3+}]_o$	$[Si]_o$	$[U]_o$	K_{Fe}	K_{Si}	K_U
TS-QA2-6-42	2.51	0.0735	1	0	0.1	0.103	-	0.076
TS-QA2-6-60 Dup	2.51	0	1	0	1	0.124	-	0.110
TS-QA2-7.5-24	2.49	0.735	1	0	0	0.735	-	-
TS-QA2-7.5-47	4.65	0.735	0	1	0.1	2.376	0.349	0.991
TS-QA2-7.5-50	4.39	0.735	0.1	1	0.1	0.539	0.188	0.295
TS-QA2-7.5-68	4.83	0.0735	0.1	1	1	2.943	0.077	0.162
TS-QA2-7.5-74	4.24	0.735	0	1	1	0.216	0.056	0.017
TS-QA2-7.5-77	4.11	0.735	0.1	1	1	0.001	0.019	0.000
TS-QA2-9-40	6.39	0.0735	0.1	0.1	0.1	2.943	0.131	1.326
TS-QA2-9-40 Dup	6.65	0.0735	0.1	0.1	0.1	2.943	0.114	1.326
TS-QA2-9-47	5.67	0.735	0	1	0.1	15.705	0.399	1.326
TS-QA2-9-59	5.80	0	0.1	1	1	0.740	0.000	0.137
TS-QA2-9-68	5.50	0.0735	0.1	1	1	0.963	0.000	0.124
TS-QA2-9-74	4.49	0.735	0	1	1	0.646	0.160	0.111
TS-QA2-9-77	4.35	0.735	0.1	1	1	0.318	0.081	0.072
TS-QA2-9-78	2.50	0.735	1	0	1	0.272	-	0.042

Data from R02TS.001 worksheet "K Values" R02JD.005, R02JD.006, and R02JD.007

7.3.2. IR analysis of solid phases

The IR analysis provided information on the functional groups present in the precipitates. From the IR bending and stretching frequencies, the solids contain Fe oxides (FeO and Fe_2O_3), uranyl, silicates, and hydroxides/water as functional groups. Examples of IR spectra and the data interpretation of samples with high levels of Fe, Si, and U are presented below.

Figure 7. IR spectrum of TS-QA2-7.5-74, a sample with 54 % Si

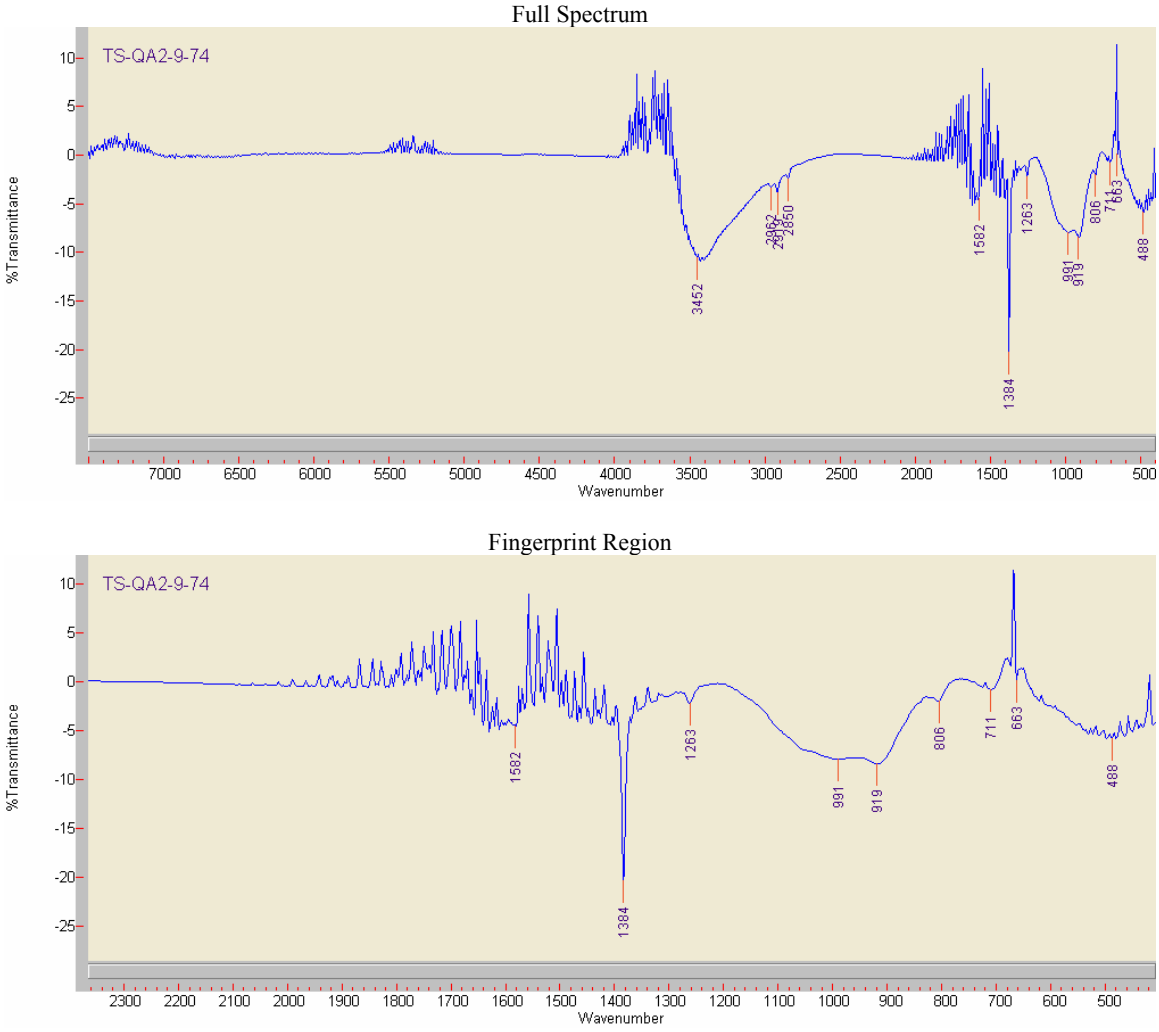

IR spectra from UCCSN-UNLV-087 vol. 1, Non-Q for information only

Table 9. IR spectrum interpretation of TS-QA2-7.5-74, a sample with 54 % Si.

Peak (cm^{-1})	Group
535	ν FeO
806	ν_1 SiO_3^{2-}
919	UO_2^{2+}
991	ν_1 CO_3^{2-}
1384	ν_1 CO_3^{2-}
1582	OH^-/H_2O
2850	Fe_2O_3
2919	Fe_2O_3
2962	Fe_2O_3
3452	OH^-/H_2O

Elemental composition: Si 54.42 %, Fe 29.77 %, U 15.81 %

IR wavenumbers from UCCSN-UNLV-087 vol. 1 and elemental composition from UCCSN-UNLV-087 vol. 2, Non-Q for information only

Figure 8. IR spectrum of TS-QA2-6-42, a sample with 86.1 % Fe.

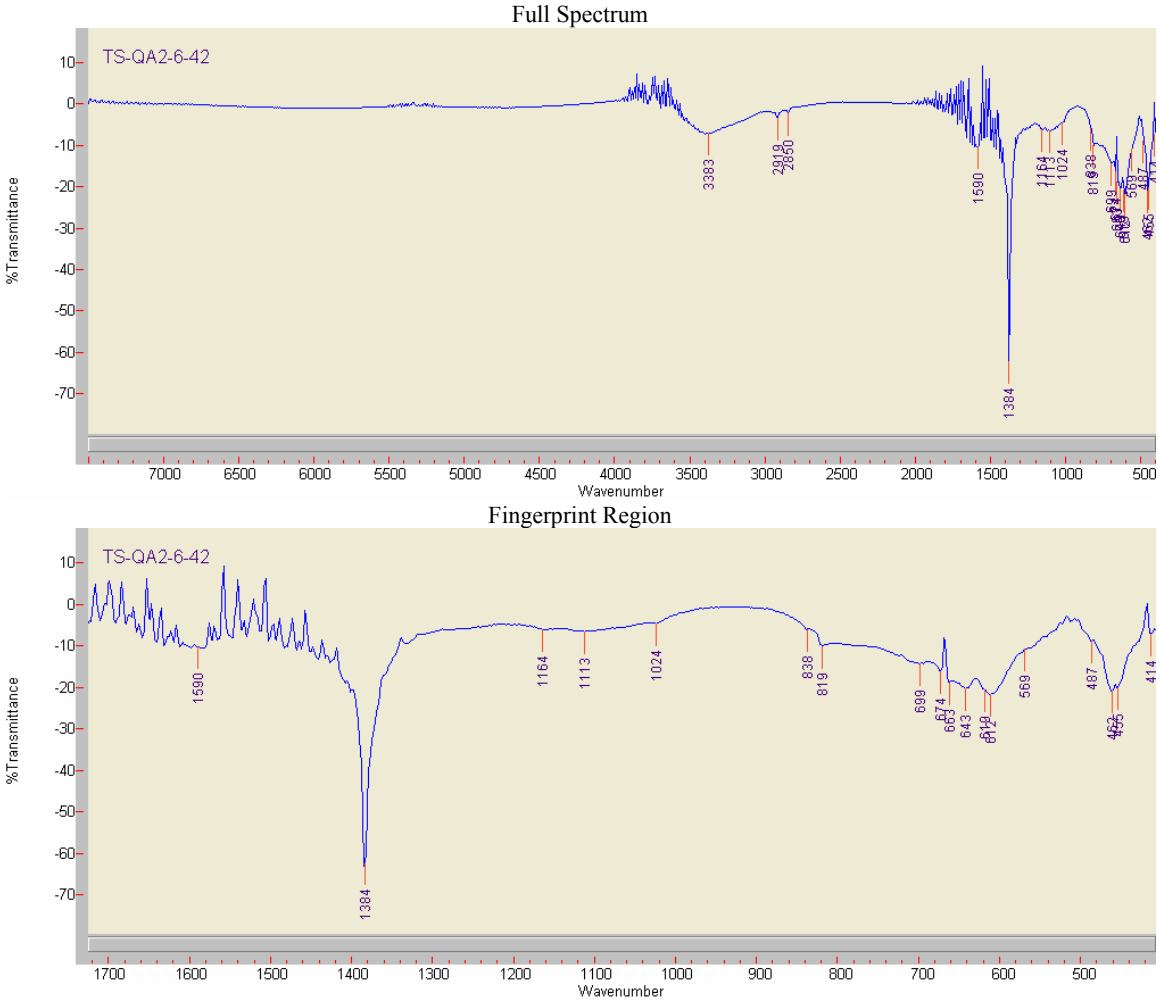

IR spectra from UCCSN-UNLV-087 vol. 1, Non-Q for information only

Table 10. IR spectrum interpretation of TS-QA2-6-42, a sample with 86.1 % Fe.

Peak (cm^{-1})	Group
569	ν FeO
1113	ν_1 CO_3^{2-}
1384	ν_3 CO_3^{2-}
1590	OH^-/H_2O
2850	Fe_2O_3
2919	Fe_2O_3
3383	OH^-/H_2O

Elemental composition: 0 % Si, 86.1 % Fe, and 6.5 % U

IR wavenumbers from UCCSN-UNLV-087 vol. 1 and elemental composition from UCCSN-UNLV-087 vol. 2, Non-Q for information only

Figure 9. IR spectrum of TS-QA2-9-40, a sample with 33 % U

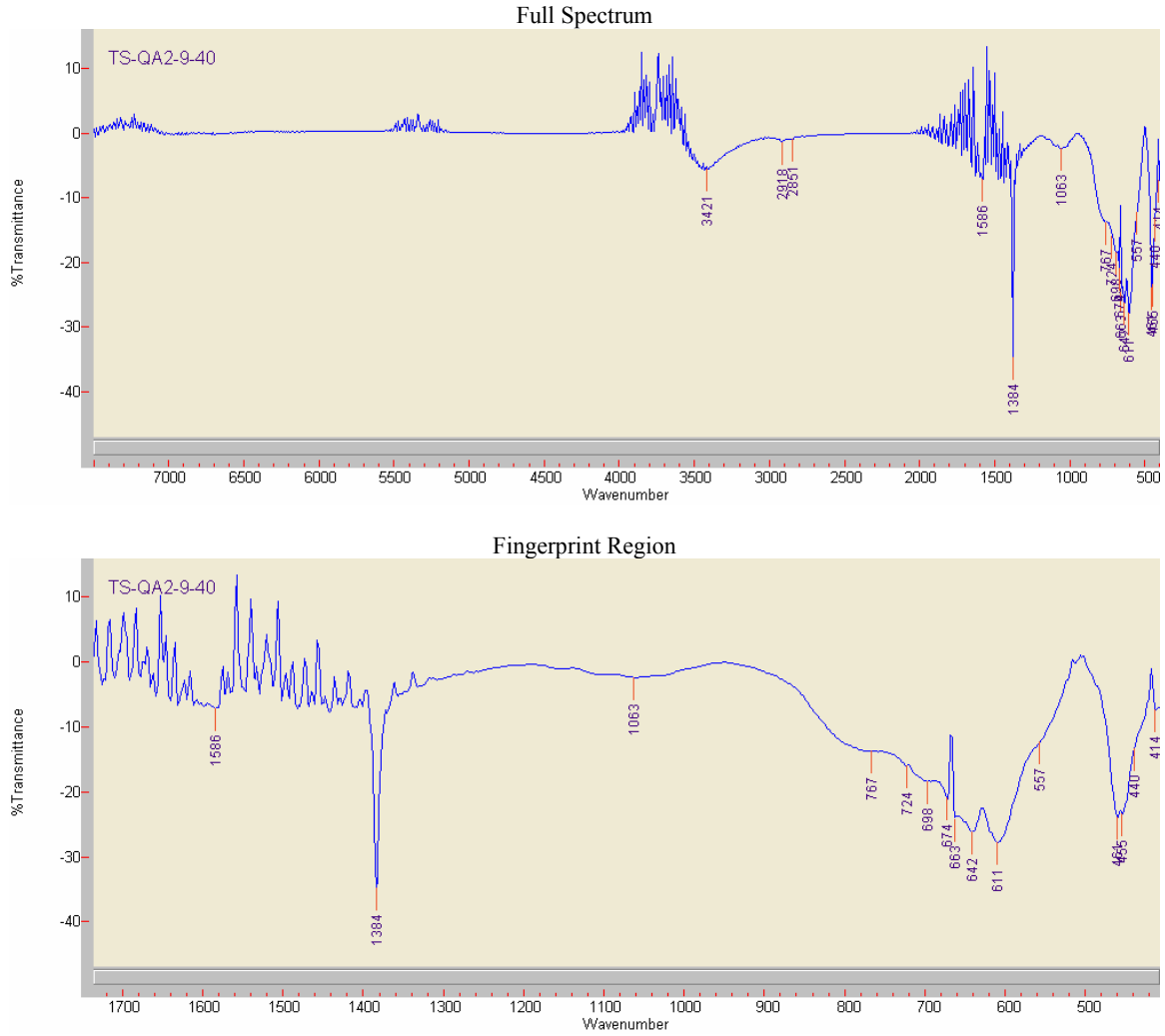

IR spectra from UCCSN-UNLV-087 vol. 1, Non-Q for information only

Table 11. IR spectrum interpretation of TS-QA2-9-40, a sample with 33.17 % U.

Peak (cm^{-1})	Group	
802	ν_1 SiO_3^{2-}	Elemental composition: Si 24.08 %, Fe 42.75 %, and U 33.17 %
904	UO_2^{2+}	
1063	ν_1 CO_3^{2-}	
1384	ν_3 CO_3^{2-}	
1585	OH^-/H_2O	
2854	Fe_2O_3	
2922	Fe_2O_3	
3383	OH^-/H_2O	

IR wavenumbers from UCCSN-UNLV-087 vol. 1 and elemental composition from UCCSN-UNLV-087 vol. 2, Non-Q for information only

7.3.3. Uranium XAFS analysis of solid phases

The solid samples examined by XAFS are TS-QA2-9-40 Dup, TS-QA2-9-47, TS-QA2-9-59, and TS-QA2-7.5-47. The elemental composition of the samples is shown in Table 12.

Table 12. Elemental composition of XAFS samples.

Sample	EDAX results (molar %)		
	Si	Fe	U
TS-QA2-9-40 Dup	24.08	42.75	33.17
TS-QA2-9-47	59.13	32.75	8.12
TS-QA2-9-59	42.85	21.92	35.23
TS-QA2-7.5-47	58.06	35.88	6.06

EDAX data from UCCSN-UNLV-087 vol. 2, Non-Q for information only

The U-L_{III} XANES spectra (Figure 10**)** of the four samples are similar. The position of the edge energy is consistent with U(VI). The presence of a shoulder at 17.19 keV indicates that U(VI) is present at the UO_2^{2+} moiety . No evidence is observed of UO_2 that can be formed from reduction of U(VI) by Fe(II) under the conditions in this study.

EXAFS spectra were extracted, k^2-weighted, and a Fourier transform performed between k = [2.5, 11.5] cm^{-1}. The Fourier transform of the data is presented in (Figure 11). The results indicate that all the samples present a peak at 1.7 Å that is characteristic of the U=O scattering and a peak around 2 Å characteristic of U-O_{eq} interaction. The difference between the sample arises around R + Δ = 3.5 Å. The TS-QA2-9-40 Dup sample exhibits a peak at 3.5 Å. This sample has the highest pH and lowest silicate concentration. Based on these conditions the role of hydrolysis in the formation of this precipitate should be larger than the other examined U containing solids. The EXAFS spectrum of TS-QA2-9-40 Dup exhibits a scattering wave function that is typical of a heavy atom. The peak was fitted using U-U contribution calculated in UO_3 with a U-U scattering at 3.64 Å. This short distance has been observed in U(VI) precipitates [31] and is characteristic of schoepite $UO_3.xH_2O$. For the other samples a U-Si interaction is needed in addition to U=O, U-O_{eq1}, U-O_{eq2} U=O (MS) and U- U for fitting. The U-Si peak is observed near 3.3 Å. The U-U interaction is observed at 3.97 Å, which indicate

presence of the core structure [U(μ-O)$_2$U]. Analysis of literature data [32] indicates that the U-U distance is characteristic of the uranium silicate phase of the uranophane group.

Co-precipitation of U(VI) with Fe oxides has already been studied [33]. In order to verify that U does not co-precipitate with Fe(II) or Fe(III) a simulation was performed. The theoretical FT of U(VI) co-precipitated with FeO and Fe_2O_3 is compared with experimental data. The theoretical spectra were simulated between k = [2.5; 11.5] Å^{-1} using the structure of FeO and Fe_2O_3 [34,35]. The σ2 values used for the simulation were taken from literature [5]. The simulated and experimental spectra are presented in Figure 12. This comparison indicates that a co-precipitation of U(VI) with FeO or Fe_2O_3 will lead to FT with a very intense contribution around 3 Å due to U-Fe scattering. This scattering is noticeably absent in the experimental EXAFS, indicating that there is no formation of a U-Fe(II,III) phase from co-precipitation.

Figure 10. XANES spectra of the four U containing samples.

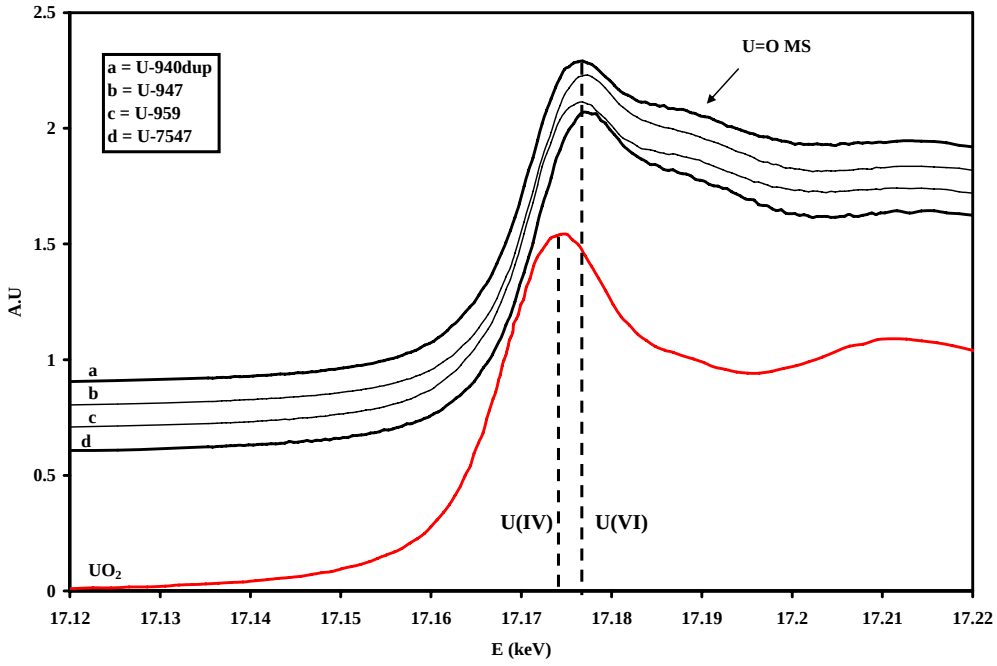

XAFS data from UCCSN-UNLV-087 vol. 1, Non-Q for information only

Figure 11. Fourier transforms of the EXAFS data.

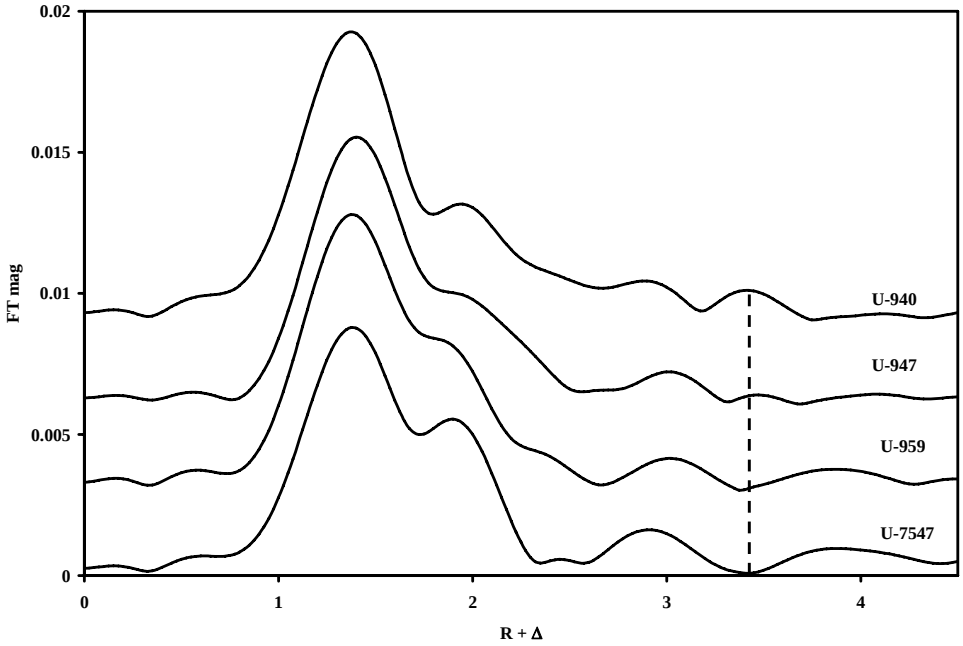

XAFS data from UCCSN-UNLV-087 vol. 1, Non-Q for information only

Figure 12. Comparison of computed U-Fe EXAFS spectra with experimental data.

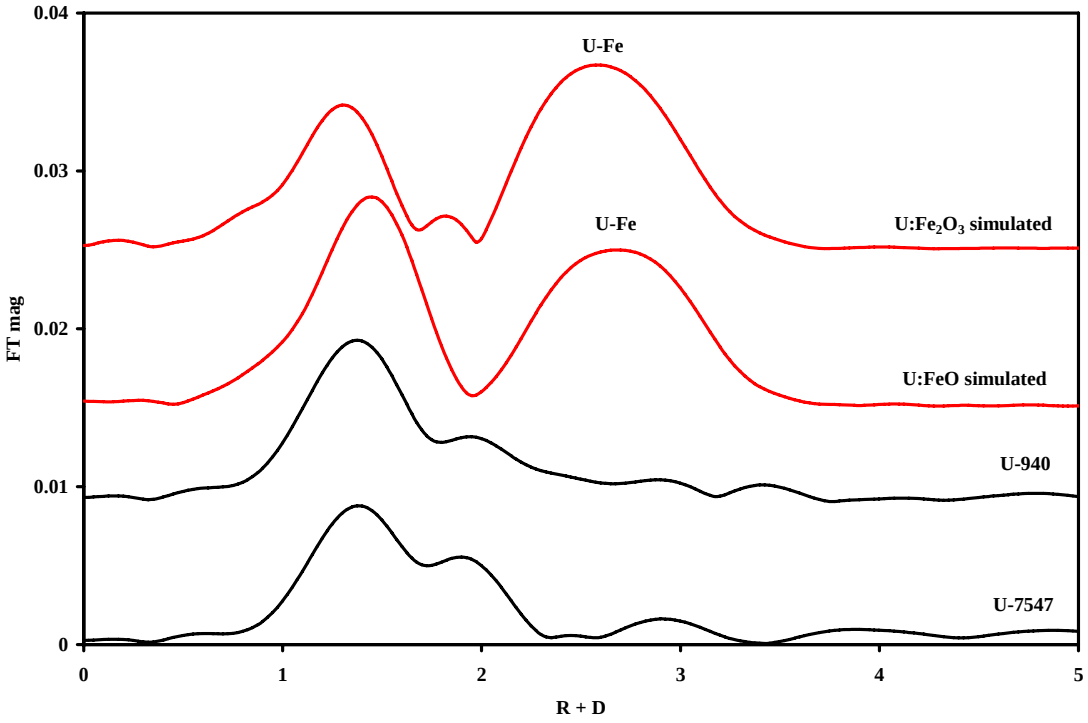

XAFS data from UCCSN-UNLV-087 vol. 1, Non-Q for information only

7.4. Results from Np(V) and Pu(VI) sorption

The solution pH varied over time but generally reached equilibrium within 5 days. Samples where Fe solid phases were in contact with the radionuclide samples exhibited equilibrium pH values between 8 and 9. This includes samples with Yucca Mountain core and iron mesh raw. Samples with only core and radionuclide showed a much larger range of pH, from 5 to 9. Solutions containing only the tracer has a low pH due to the acidity of the stock solutions. The pH conditions for the samples are provided in Table 13 and table 14.

Table 13. Equilibrium solution pH for Np(V) sorption experiments.

Sample	Solid	Solution phase	Equilibrium pH
JD-QA3-13	Np spike (no solid phase)	DI H_2O	2.32
JD-QA3-14	Np spike(no solid phase)	1 mM Si	2.46
JD-QA3-15	Np spike(no solid phase)	J-12	2.50
JD-QA3-25	Np spike, Fe	DI H_2O	8.03
JD-QA3-26	Np spike, Fe	1 mM Si	8.70
JD-QA3-27	Np spike, Fe	J-12	8.91
JD-QA3-37	core, Np spike	DI H_2O	5.90
JD-QA3-38	core, Np spike	1 mM Si	7.18
JD-QA3-39	core, Np spike	J-12	7.28
JD-QA3-49	core, Np spike, Fe	DI H_2O	8.23
JD-QA3-50	core, Np spike, Fe	1 mM Si	8.02
JD-QA3-51	core, Np spike, Fe	J-12	8.40

Data from R02JD.012

Table 14. Equilibrium solution pH for Pu(VI) sorption experiments.

Sample	Solid	Solution phase	Equilibrium pH
JD-QA3-16	Pu spike (no solid phase)	DI H_2O	3.24
JD-QA3-17	Pu spike (no solid phase)	1 mM Si	8.14
JD-QA3-18	Pu spike (no solid phase)	J-12	8.12
JD-QA3-28	Pu spike, Fe	DI H_2O	8.00
JD-QA3-29	Pu spike, Fe	1 mM Si	9.39
JD-QA3-30	Pu spike, Fe	J-12	8.50
JD-QA3-40	core, Pu spike	DI H_2O	8.43
JD-QA3-41	core, Pu spike	1 mM Si	8.68
JD-QA3-42	core, Pu spike	J-12	8.44
JD-QA3-52	core, Pu spike, Fe	DI H_2O	8.86
JD-QA3-53	core, Pu spike, Fe	1 mM Si	9.07
JD-QA3-54	core, Pu spike, Fe	J-12	8.71

Data from R02JD.012

The solution activity of Np and Pu shows a decrease with time for all samples (Figure 13 and Figure 14). This indicates sorption is occurring. The small degree decrease in dissolved tracer in samples without a solid phase is due to sorption onto the container wall.

Figure 13. $^{237}Np(V)$ sorption to Yucca Mountain core and Fe in DI water, 0.1 M SiO_3^{2-}, and J-12 groundwater.

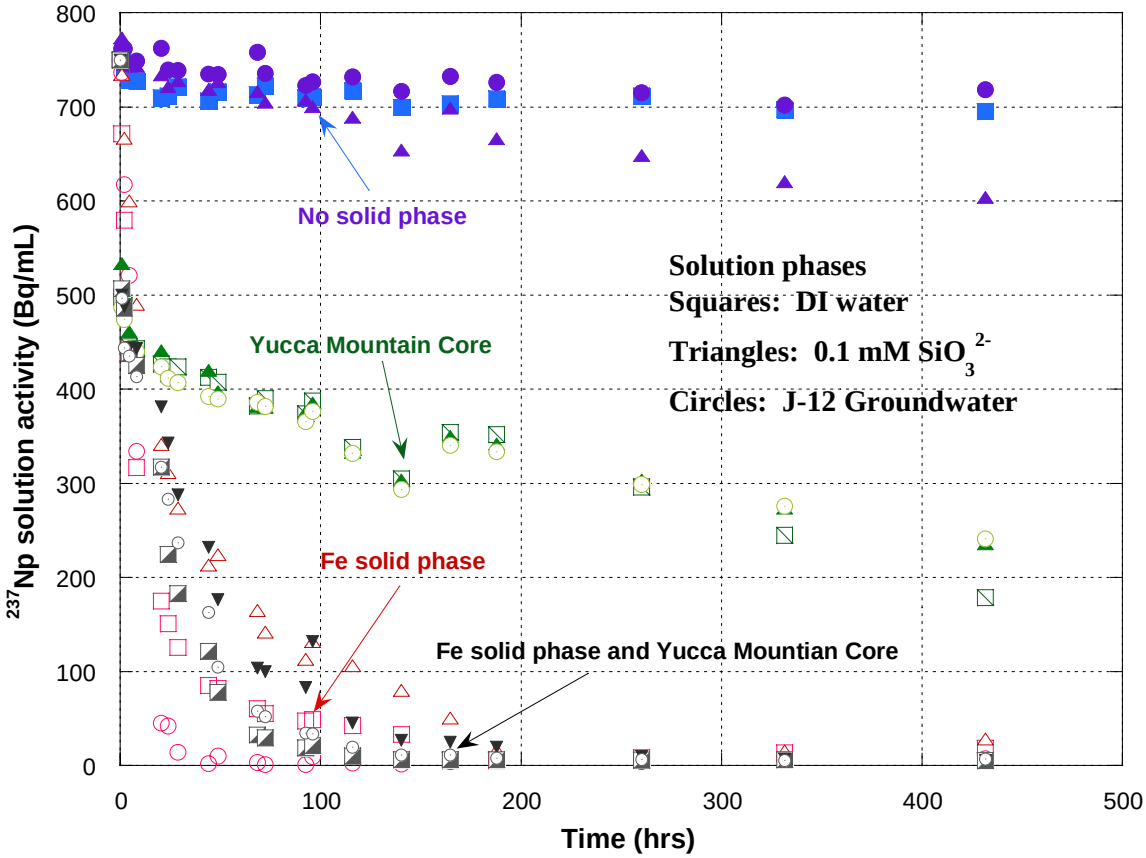

Data from R02TS.002 and R02JD.13

The Np data indicate a clear conclusion: Fe drives the formation of sorbed species. The dramatic difference between Np sorption onto Yucca Mountain core in the presence and absence of Fe metal shows the importance of this species for the retention of Np. In the samples without solid phase the silicate-containing solution displays the largest degree of sorption. The pH of this solution is 2.5 (Table 13), which can induce the precipitation of the silicates as SiO_2, based on speciation calculations, on the container surface and thereby provide extra sorption sites for Np.

The Pu(VI) sorption data show the importance of silicate in its environmental speciation. In all cases the solution containing 0.1 mM SiO_3^{2-} impedes the sorption of Pu species. The most dramatic case is for sorption to the Fe metal, in which solutions without silicate rapidly sorb Pu. There is a difference in solution pH; the silicate solution is at 9.4 and the other solutions are between pH 8 and 8.5. This result is consistent with the literature on the formation of Pu silicates above pH 9 [21].

Figure 14. ^{239}Pu(VI) sorption to Yucca Mountain core and Fe in DI water, 0.1 M SiO_3^{2-}, and J-12 groundwater.

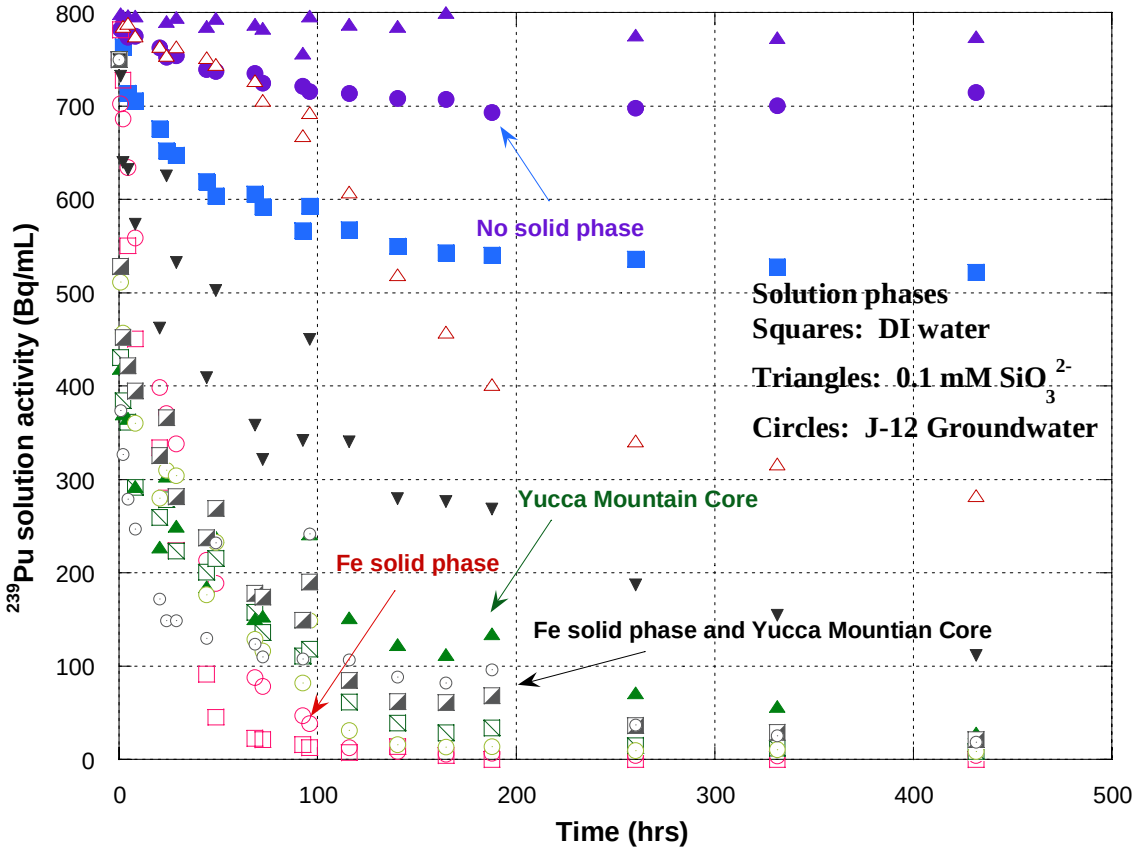

Data from R02TS.002 and R02JD.13

7.5. Conclusions Based on Q Data

The conclusions supported by QA data are listed below. These conclusions are drawn from the solution phase measurements for the precipitation and sorption experiments. Precipitation experiments conclusions:

- From the evaluation of K_U, the largest values, representing the highest relative sorbed uranium concentration, are found near pH 7. These conditions are independent of other solution ion concentrations. At this pH uranium hydrolysis is a dominate factor in speciation. Furthermore, the largest K_U values occur at the lowest examined U concentration of 0.1 mM. Silicates show an importance in forming uranium precipitates near a final pH of 5.
- No correlation is observed between the solid and solution phase speciation of Fe and U from the precipitation experiments based on the examination of K_{Fe} and K_U.
- A relationship between the solid and solution species between Si and U is observed from the relationships between K_{Si} and K_U. The slope of K_U against K_{Si} is shown to vary with the total initial uranium concentration. When 1 mM uranium is examined, the slope is 0.84 ± 0.10while under 0.1 mM uranium the

slope increases to 1.5± 0.22 This trend indicates that concentrations of uranium below 0.1 mM should have an even larger dependence on silicate at its J-13 concentration, with the degree of uranium precipitation strongly influenced by the behavior of silicate.

Sorption experiment conclusions:

- The solution activity of Np and Pu shows a decrease with time for all samples. This indicates sorption is occurring, even to a small degree in samples without a solid phase due to interaction with the container wall.
- The Np data show a clear sorption trend correlated to the presence of an iron metal solid phase, which is demonstrated by the dramatic difference between Np sorption onto Yucca Mountain core in the presence and absence of Fe metal. In the samples without solid phase, the silicate containing solution displays the largest degree of sorption due silicate precipitation which was visually observed. The behavior is different form the precipitation experiment which the presences of Fe ions in solution did not have a strong impact on the formation of Np solids.
- The Pu sorption data shows the importance of silicate in its environmental speciation, a result supported by literature reports of the high stability of plutonium silicate. In all solutions containing 0.1 mM SiO_3^{2-} the formation of sorbed Pu species is impeded. The most dramatic case is the sorption to Fe metal, in which solutions without silicate rapidly sorb Pu.

7.6. Summary of Observations Based on Non-Q Data

Summary of observations for the solid phases from precipitation experiments are listed below.

- From the EDAX analysis the highest Si percentage in precipitates was near 50 mol %. The seven samples in this range all had an initial silicate concentration of 1 mM . All contained uranium. The final pH of these solutions was below 5.75.
- For Fe EDAX analysis, most of the samples examined have atomic Fe elemental percentages between 20 % and 30 %. The highest Fe percentages detected were between 80 % and 90 %. These high Fe containing precipitates result from solution with total Fe concentration at or above 1 mM and a final pH near 2.5.
- Uranium EDAX studies showed that the precipitates reach an atomic elemental percentage maximum of 35 ± 2 % U, with most of the samples exhibiting around 10 % U. The five high U samples have either high K_U values or have 1 mM solution phase U concentration in the presence 1 mM silicate. The formation of the U-silicate solids forms an equilibrium near pH 5.
- The IR analysis provided information on the functional groups present in the precipitates. The solids are shown to contain Fe oxides (FeO and Fe_2O_3), uranyl, silicates, sorbed water, and hydroxide as functional groups.
- XANES analysis indicates that the uranium is present as the UO_2^{2+} moiety in the examined samples. No reduced uranium solid species are observed, even in the presence of Fe^{2+}.
- The EXAFS analysis shows $UO_3 \bullet xH_2O$ is formed with 0.1 mM Fe(II,III) and 0.1mM Si at pH 6.65. These results confirm the importance of uranium hydrolysis even in the presence of other solution species, well documented in the literature.

A uranium–silicon phase was detected by the U-U interaction at 3.97 Å, characteristic of the uranophane group, whose minerals include sklodowskite, α-uranophane, and boltwoodite. This precipitate equilibrated at pH 4.5

- EXAFS simulation study indicates that the incorporation of U(VI) in FeO or Fe_2O_3 structure does not occur in the studied samples.

8. References

---

1. Runde, Wolfgang; Conradson, Steve D.; Wes Efurd, D.; Lu, NingPing; VanPelt, Craig E.; Tait, C. Drew: .Solubility and sorption of redox-sensitive radionuclides (Np, Pu) in J - 13 water from the Yucca Mountain site: comparison between experiment and theory. Applied Geochemistry (2002), 17(6), 837-853.
2. Colloid-Facilitated Transport of Low-Solubility Radionuclides: A Field, Experimental, and Modeling Investigation, Editors Annie B. Kersting and Paul W. Reimus, UCRL-ID-149688 (http://www.llnl.gov/tid/lof/documents/pdf/246025.pdf)
3. Choppin, Gregory R : Actinide speciation in the environment. Radiochimica Acta (2003), 91(11), 645-649.
4. Kim, J.I.: Chemical Behavior of Transuranic Elements in Natural Aquatic Systems, Handbook on the Physics and Chemistry of the Actinides, A.J. Freeman and C. Keller Eds., Elsevier Publishers, 1986, 413-455.
5. Von Gunten, H.R., and Benes, P.: Speciation of Radionuclides in the Environment. Radiochim. Acta, **69**, 1-29 (1995).
6. Silva, R.J. and Nitsche, H.: Actinide Environmental Chemistry, Radiochim. Acta, **70/71**, 377-396 (1995).
7. Moulin, V and Moulin, C.: Radionuclide Speciation in the Environment: A Review. Radiochim. Acta, **89(11-12)**, 773-778 (2001).
8. J. Plaue and K.R. Czerwinski, Actinide Speciation in Environmental Remediation, J. Nucl. Sci. Supp 3, 461-465 (2002).
9. Duff, M. C.; Hunter, D. B.; Triay, I. R.; Bertsch, P. M.; Reed, D. T.; Sutton, S. R.; Shea-McCarthy, G.; Kitten, J.; Eng, P.; Chipera, S. J.; Vaniman, D. T.: Mineral associations and average oxidation states of sorbed Pu on tuff. Environmental Science and Technology (1999), 33(13), 2163-2169.
10 Mincher, Bruce J.; Fox, Robert V.; Cooper, D. Craig; Groenewold, Gary S.: Neptunium and plutonium sorption to Snake River plain, Idaho soil**.** Radiochimica Acta (2003), 91(7), 397-401.
11 Combes, Jean Marie; Chisholm-Brause, Catherine J.; Brown, Gordon E., Jr.; Parks, George A.; Conradson, Steven D.; Eller, P. Gary; Triay, Ines R.; Hobart, David E.; Miejer, Arend: EXAFS spectroscopic study of neptunium(V) sorption at the α-iron hydroxide oxide (α-FeOOH)/water interface. Environmental Science and Technology (1992), 26(2), 376-82.
12. Kohler, M.; Honeyman, B. D.; Leckie, J. O.: Neptunium (V) sorption on hematite (α-Fe_2O_3) in aqueous suspension. The effect of CO_2. Radiochimica Acta (1999), 85(1-2), 33-48.

13. Khasanova, A. B.; Shcherbina, N. S.; Kalmykov, St. N.; Novikov, A. P.; Clark, S. B.: Neptunium(V) sorption by α-FeOOH and γ-Fe_2O_3. AIP Conference Proceedings (2003), 673(Plutonium Futures--The Science), 357-359.
14. Tochiyama, O.; Yamazaki, H.; Mikami, T.: Sorption of neptunium(V) on various aluminum oxides and hydrous aluminum oxides. Radiochimica Acta (1996), 73(4), 191-198.
15. Del Nero, M.; Ben Said, K.; Made, B.; Clement, A.; Bontems, G.: Effect of pH and carbonate concentration in solution on the sorption of neptunium(V) by hydrargillite. Application of the non-electrostatic model. Radiochimica Acta (1998), 81(3), 133-141.
16. Turner, David R.; Pabalan, Roberto T.; Bertetti, F. Paul.: Neptunium(V) sorption on montmorillonite: an experimental and surface complexation modeling study. Clays and Clay Minerals (1998), 46(3), 256-269.
17. Bertetti, F. Paul; Pabalan, Roberto T.; Almendarez, Michael G: Studies of neptuniumV sorption on quartz, clinoptilolite, montmorillonite, and α-alumina. Adsorption of Metals by Geomedia. Editor(s): Jenne, Everett A. Publisher: Academic, San Diego, CA.(1998), 131-148.
18. Kohler, M.; Wieland, E.; Leckie, J.O. Metal-ligand-surface interactions during sorption of uranyl and neptunyl on oxides and silicates. Water-Rock Interact., Proc. Int. Symp., 7th, Editor(s): Kharaka, Yousif K.; Maest, Ann S (1992), 1 51-4.
19. Lomenech, C.; Drot, R.; Simoni, E.: Speciation of uranium(VI) at the solid/solution interface: Sorption modeling on zirconium silicate and zirconium oxide. Radiochimica Acta (2003), 91(8), 453-461.
20. Paulus, J. M.; Bontems, G.; Schleiffer, J. J.: Neptunium(V and VI) exchange between silicate gels and aqueous solutions. Applied Clay Science (1992), 7(1-3), 71-8.
21. Shilov, V. P.; Fedoseev, A. M: .Solubility of Pu(IV) in Weakly Alkaline Solutions (pH 9-14) Containing Silicate Anions. Radiochemistry, (2003), 45(5), 491-494.
22. Fortner, J. A.; Mertz, C. J.; Bakel, A. J.; Finch, R. J.; Chamberlain, D. B.: Plutonium silicate alteration phases produced by aqueous corrosion of borosilicate glass. Materials Research Society Symposium Proceedings (2000), 608(Scientific Basis for Nuclear Waste Management XXIII), 739-744.
23. Burakov, B. E.; Anderson, E. B.; Zamoryanskaya, M. V.; Yagovkina, M. A.; Strykanova, E. E.; Nikolaeva, E. V.: Synthesis and study of 239Pu-doped ceramics based on zircon, (Zr,Pu)SiO4, and hafnon, (Hf,Pu)SiO4. Materials Research Society Symposium Proceedings (2002), 663(Scientific Basis for Nuclear Waste Management XXIV), 307-313.
24. Dzombak, D.A. and FM.M. Morel (1990). *Surface Complexation Modeling: Hydrous Ferric Oxide*. Wiley-Interscience (New York).
25. Davis, J.A., Coston, J.A., Kent, D.B. and Fuller, C.C. (1998). Application of the surface complexation concept to complex mineral assemblages. *Environ. Sci. Technol.,* **32**, 2820-2828.
26. Honeyman, B.D. (1984). *Cation and Anion Adsorption in Binary Mixtures of Adsorbents: An Investigation of the Concept of Adsorptive Additivity.* Ph.D. Dissertation, Stanford University.

27. Turner, D. R.; Bertetti, F. P.; Pabalan, R.T.: Role of radionuclide sorption in high-level waste performance assessment: approaches for the abstraction of detailed models. SSSA Special Publication **59**(Geochemistry of Soil Radionuclides), 211-252 (2002).
28. W.J. Moore: Basic Physical Chemistry Prentice Hall, 1983 pgs. 159-166.
29. G. Curran, W. Rattray, and K.R. Czerwinski, Solubility of Thorium from Th_3UO_8 and $ZrTh_3UO_{10}$ Ceramics, Radiochimica Acta **91(4)**, 203-209, (2003).
30. Ogard, A. E.; Kerrisk, J. F. "Groundwater Chemistry Along the Flow Path between a Proposed Repository Site and the Accessible Environment," Los Alamos National Laboratory, 1984.
31. Allen, P. G.; Shuh, D. K.; Bucher, J. J.; Edelstein, N. M.; Palmer, C. E. A.; Silva, R. J.; Nguyen, S. N.; Marquez, L. N.; Hudson, E. A.: Determinations of uranium structures of EXAFS : schoepite and other U (VI) oxide precipitates. Radiochimica Acta (1996), 75(1), 47-53.
32. Catalano, Jeffrey G.; Heald, Steven M.; Zachara, John M.; Brown, Gordon E., Jr. Spectroscopic and Diffraction Study of Uranium Speciation in Contaminated Vadose Zone Sediments from the Hanford Site, Washington State. Environmental Science and Technology (2004), 38(10), 2822-2828.
33. Duff, Martine C.; Coughlin, Jessica Urbanik; Hunter, Douglas B.: Uranium co-precipitation with iron oxide minerals. Geochimica et Cosmochimica Acta (2002), 66(20), 3533-3547.
34. Antic, B.;Kremenovic, A.;Nikolic, A.S.;Stoiljkovic, M:. Cation distribution and size-strain microstructure analysis in ultrafine Zn-Mn Ferrites obtained from acetylacetonato complexes J. Phys. Chem. B . (2004), 108(34), 12646
35. Fjellvag, H.;Gronvold, F.;Stolen, S.;Hauback, B.C.: On the crystallographic and magnetic structures of nearly stoichiometric iron monoxide. Journal of Solid State Chemistry. (1996), 124, 5.